Catalysis Today 165 (2011) 96–105

Contents lists available at ScienceDirect

Catalysis Today

journal homepage: www.elsevier.com/locate/cattod

Effect of Pd surface structure on the activation of methyl acetate

Lijun Xu, Ye Xu*

Center for Nanophase Materials Sciences, Oak Ridge National Laboratory, Oak Ridge, TN 37831, USA

ARTICLE INFO

Article history:
Received 1 October 2010
Received in revised form
30 November 2010
Accepted 3 December 2010
Available online 16 January 2011

Keywords:
Ester
Methyl acetate
Palladium
Selectivity
Step/kink
DFT

ABSTRACT

The activation of methyl acetate (CH_3COOCH_3) has been studied using periodic density functional theory calculations to probe the effect of Pd surface structure on this reaction. The adsorption of methyl acetate, dehydrogenated derivatives including enolate (CH_2COOCH_3) and methylene acetate (CH_3COOCH_2), and dissociation products including acetate, acetyl, ketene, methoxy, formaldehyde, CO, C, O, and H; and the C–H and RCO–OR′ C–O bond dissociation in methyl acetate, enolate, and methylene acetate, are calculated on Pd(1 1 1) terrace, step edge, and kink; and on Pd(1 0 0) terrace and step edge. The adsorption of most species is not strongly affected from (1 1 1)- to (1 0 0)-type surfaces, but is clearly enhanced by step/kink compared to the corresponding terrace. For a given reactant, going both from terrace to step edge and from (1 1 1)- to (1 0 0)-type surfaces stabilizes the transition states of C–O bond dissociation steps. Going from terrace to step edge also stabilizes the transition states of C–H bond dissociation steps, but going from (1 1 1)- to (1 0 0)-type surfaces does not clearly do so. Our results suggest that compared to the Pd(1 1 1) terrace, the Pd(1 0 0) terrace is more selective for the C–O bond dissociation that is desirable for alcohol formation, whereas step edges are more selective for C–H bond dissociation.

1. Introduction

The hydrogenolysis of esters has been one of the key industrial processes for producing alcohols, e.g. ethanol from methyl and ethyl acetate; fatty alcohols from natural fats and oils; and diols from di-esters for polymer synthesis [1–4]. With growing interest in producing fuels and value-added chemicals from alternative biomass feedstock [5–8], catalytic hydrogenolysis may become an important step in the conversion and utilization of yet other esters. Because of the industrial interest in ester hydrogenolysis, many kinetic experiments have been reported over several decades for various esters, the majority of which being aliphatic esters [1,9–19] Turek and Trimm provided a comprehensive review of the catalytic hydrogenolysis of esters to alcohols [4]. The reaction is traditionally catalyzed by copper or copper-based compounds, which have good activity and selectivity for alcohols under high temperature and hydrogen pressure (500–700 K; 200–300 bar). Two decades ago some studies emerged indicating that Pt-group metals, including Rh, Pd, and Ru, can reduce the required temperature and pressure for ester hydrogenolysis, although by themselves these metals substantially favor the production of hydrocarbons over alcohols [11–13,15,20]. Alloying with Fe [11], Sn [12,20,21], and Zn [11,13,15,19] enhances the selectivity for alcohols.

The ability to avoid hydrocarbon production is important to the development of more efficient and versatile catalysts for ester hydrogenolysis. So far, however, the factors that govern the selectivity remain poorly understood. The large body of experimental work in the literature primarily involves the analysis of overall kinetics, with few studies exploring the atomic-level mechanistic details of metal-catalyzed ester hydrogenolysis using surface science techniques or computational modeling [18,22–29], even for simple aliphatic esters on Pd, a well-known hydrogenation catalyst [30]. Wehner and Gustafson estimated the apparent E_a for methyl acetate (MA) hydrogenolysis to be 14.5 kcal/mol on Pd/ZnO catalysts under elevated temperature and hydrogen pressure [13], although the active phase of Pd/ZnO may not be Pd but Pd-Zn alloys [15] because Pd/Al_2O_3 has nearly zero ethanol selectivity [11]. Lambert and co-workers examined the adsorption of acetic acid, a related molecule, on Pd(1 1 1) in vacuuo and reported that acetate began to decompose non-selectively at 230 K [31]. The non-selective decomposition of MA on a clean Pd(1 1 1) surface should not require a higher temperature and would therefore imply a small activation barrier. The apparent E_a for MA hydrogenolysis on Cu/SiO_2 has been reported to be higher, at 1.0–1.3 eV [11,32].

Recently, we have performed density functional theory (DFT) calculations to investigate the reactivity of MA and its derivatives on Pd(1 1 1) [33]. In contrast to Cu, on which acetates are thought to undergo direct C–O bond dissociation [9,10,18], the reactivity of MA on clean Pd(1 1 1) is dominated by dehydrogenation, which occurs before the dissociation of any C–O bond. Because extensive dehydrogenation can lead to C–C bond scission that is

* Corresponding author at: 1 Bethel Valley Road, P.O. Box 2008, MS-6493, Oak Ridge, TN 37831-6493, USA. Fax: +1 865 574 1753.
E-mail address: xuy2@ornl.gov (Y. Xu).

0920-5861/$ – see front matter © 2010 Elsevier B.V. All rights reserved.
doi:10.1016/j.cattod.2010.12.021

undesirable in alcohol production [21,34–36], our findings suggest that the selectivity for alcohol in the hydrogenolysis of MA and likely other aliphatic esters is limited by, among other factors, C–H vs. C–O bond dissociation activities in the ester molecules on Pd.

It is well known that the activity of a number of dissociation reactions, e.g. CO [37–39], N_2 [40,41], NO [42–44], and C–C bonds in alkanes [45–47], are sensitive to metal surface structure, which have important consequences for technological reactions such as ammonia synthesis, NO reduction, methanation reaction, and Fischer–Tropsch synthesis. It has been shown that open surfaces and under-coordinated atoms on metals possess higher-lying d states or more favorable local geometry than the prevalent close-packed facet (e.g. (1 1 1) and (0001) facets of fcc and hcp metals, respectively), thereby appreciably lowering the bond-breaking barriers [41,48–53].

On the other hand, the effect of metal surface structure on reaction selectivity, especially in multi-step reactions involving larger molecules, is less well explored. Wang and Liu reported that the electro-oxidation of ethanol is less efficient on Pt(1 1 1) than on Pt(1 0 0) and step edges because on Pt(1 1 1) the dehydrogenation of intermediates such as acetyl is more difficult but the oxidation of acetyl is more facile, resulting in low C–C bond scission activity and instead poisoning by acetate [35]. Using DFT calculations and elegant synthesis Christopher and Linic showed that Ag(1 0 0) is more selective than Ag(1 1 1) for ethylene epoxidation because the activation barrier that an oxametallacycle intermediate must overcome to form ethylene oxide is 0.1 eV lower than that for forming acetaldehyde on Ag(1 0 0), but the two are identical on Ag(1 1 1) [54,55]. Goodman and co-workers found the rate of vinyl acetate formation from ethylene acetoxylation on Pd-Au surface alloys to be consistently higher on Au(1 0 0) than on Au(1 1 1), and attributed this phenomenon to the spacing between neighboring Pd monomers on Au(1 0 0) being more favorable for C–O coupling than that on Au(1 1 1) [56,57]. These intriguing findings suggest that the surface structure of catalysts can have a subtle but clear influence on the selectivity of a reaction and needs to be taken into account in the design and engineering of new catalytic materials.

Previously, Liu and Hu reported that at step edges of Pd(1 1 1) C–H bond dissociation in CH_4 is enhanced primarily due to local electronic effect, but the dissociation of molecular CO benefits substantially from the geometric effect of dissociating against the edge [49]. For MA hydrogenolysis, it is unknown how different Pd surface structures facilitate C–O and C–H bond dissociation differentially in the same molecule, which, if true, may impart different surface structures different reaction selectivites. In this contribution, we investigate C–O and C–H bond dissociation in MA on the Pd(1 0 0) terrace; at the edges of Pd(1 1 1) and Pd(1 0 0) terraces; and at a kink site at the edge of a Pd(1 1 1) terrace. We focus on the (1 1 1) and (1 0 0) facets because an ideal cuboctahedral particle of an fcc metal exposes only (1 1 1) and (1 0 0) terraces, joined by edges and vertices, on its surface. The atoms in the (1 0 0) facet are arranged in square instead of the hexagonal symmetry of the (1 1 1) facet. The relative concentration of edges and kinks inevitably increases with shrinking particle size. In the following sections, we first summarize the adsorption of key species on the different Pd surfaces, and then investigate C–O and C–H bond dissociation in MA and its dehydrogenated derivatives, enolate and methylene acetate. A comparison of these different surface structures suggests that relative to Pd(1 1 1) terrace, Pd(1 0 0) terrace is more selective for C–O dissociation whereas step edge is more selective for C–H dissociation, which implies that the concentration of (1 0 0) facets should be maximized and that of step/kink sites minimized for Pd catalyst particles used for ethanol production via MA hydrogenolysis.

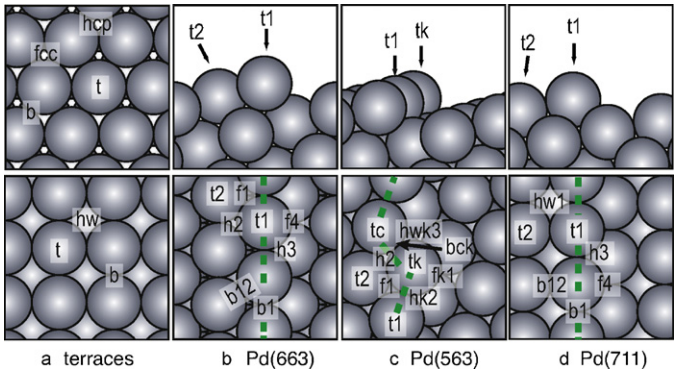

Fig. 1. The different Pd surface structures employed in this study: (a) top views of Pd(1 1 1) (upper) and Pd(1 0 0) (lower) terraces; and side (upper) and top (lower) views of (b) Pd(6 6 3); (c) Pd(5 6 3); and (d) Pd(7 1 1). Dashed lines indicate the step edge position; atoms along and to the left of the dashed lines are inside the edge (same in figures below). Selected high-symmetry sites are labeled; t = top; b = bridge; f/h = fcc/hcp; hw = hollow. k indicates kink, and c indicates corner.

2. Methods

Periodic DFT calculations are performed using the Vienna *Ab initio* Simulation Package (VASP) [58–60] in the generalized gradient approximation (GGA-PBE [61]). The core electrons are described by the projector augmented wave (PAW) method [62], and the Kohn–Sham valence states are expanded in plane wave basis sets up to 400 eV. A first-order Methfessel–Paxton scheme [63] is used to smear the electronic states with a temperature of 0.1 eV. All total energies are extrapolated back to 0 K. The surface Brillouin zone is sampled with a $3 \times 3 \times 1$ Monkhorst–Pack *k*-point grid. Density of states (DOS) calculations use a $5 \times 5 \times 1$ Monkhorst–Pack *k*-point grid and the tetrahedron method with Blöchl corrections [64] for determining the occupancies of electronic states instead.

The equilibrium lattice constant of bulk fcc Pd is calculated to be 3.953 Å, in close agreement with the experimental value (3.89 Å) [65]. Pd(1 1 1) and Pd(1 0 0) terraces are each modeled by a four-layer slab with a (3×3) surface unit cell leading to a coverage of 1/9 ML per adsorbate (see Fig. 1 for the different surface models). Adjacent slabs in the *z* direction are separated by a 16-Å thick vacuum. The step edges of Pd(1 1 1) and (1 0 0) terraces are represented by Pd(6 6 3) and Pd(7 1 1) respectively, each of which features a monoatomic step and is modeled by a three-layer (in the direction normal to the terrace) slab with the terrace being four atoms wide and four atomic rows deep, for a total of 48 atoms in each unit cell. Pd(5 6 3) is used to represent a (1 1 1) terrace terminated by a kinked monoatomic step. Likewise it is modeled by a three-layer (in the direction normal to the terrace) slab with the terrace being three atoms wide and four atomic rows deep, for a total of 36 atoms in the unit cell. For all the stepped slabs, neighboring images in the *z* direction are separated by a 14-Å thick vacuum. In the follow sections we refer to Pd(1 1 1), (6 6 3), and (5 6 3) collectively as (1 1 1)-type surfaces, and Pd(1 0 0) and (7 1 1) as (1 0 0)-type surfaces.

The adsorption energy (E_{ads}) for an atom or molecule adsorbed on a Pd surface is calculated as follows:

$$E_{ads} = E_{molecule/Pd} - E_{molecule} - E_{Pd}$$

where $E_{molecule/Pd}$ is the total energy of a Pd slab with an adsorbate, $E_{molecule}$ is the energy of the neutral adsorbate isolated in the gas phase, and E_{Pd} is the energy of the Pd surface without any adsorbate. A more negative adsorption energy therefore means stronger adsorption. All Pd atoms are fixed in their bulk positions. The effect of surface relaxation is explored by relaxing the top two metal layers of the Pd(1 1 1) and Pd(1 0 0) slabs and the top metal layer of the stepped slabs, which includes the row of atoms directly beneath the

step edge [49,53]. Geometry optimization is converged to 0.01 eV/Å for each relaxed atomic degree of freedom.

The minimum-energy reaction paths and transition states (TSs) for elementary steps are calculated using the climbing-image nudged elastic band (CI-NEB) method [66,67] and the dimer method [68–70]. Each TS is verified to possess a single imaginary vibrational frequency. The activation barrier for an elementary step is defined to be the difference between the energies of the TS and the initial state (IS), which will be the adsorbed reactant unless noted otherwise: $E_a = E_{TS} - E_{IS}$. The reaction energy is defined to be the difference between the energies of the product or final state (FS) and the IS: $\Delta E = E_{FS} - E_{IS}$. The energy of the FS is calculated with the dissociated fragments in their most stable configurations at infinite separation from each other.

3. Results and discussion

3.1. Adsorption of molecular and atomic species

3.1.1. Methyl acetate and derivatives

Molecular MA (RCOOR′, with R = R′ = CH_3; CH_3COO- is designated as the acetate end and $-OCH_3$ designated as the methoxy end) prefers the *cis* to the *trans* configuration by 0.30 eV in the gas phase. Likewise, the preferred adsorption mode of MA on the various Pd surfaces at the given low coverage involves the cis configuration bonding through the carbonyl oxygen to a single Pd atom, with the molecular plane perpendicular to the surface (Fig. 2). Alternate adsorption states have been found to be less stable on Pd(1 1 1) [33]. Step edge and kink sites lower MA adsorption energy from ca. −0.2 eV on the terraces to ca. −0.5 eV (Table 1).

The dehydrogenation of MA produces enolate (CH_2COOCH_3, abbreviated as ENL) and methylene acetate (CH_3COOCH_2, abbreviated as MeA), both of which adsorb strongly through the unsaturated carbon to a single Pd atom. The adsorption energies of the two species are similar and vary little from (1 1 1) to (1 0 0) terraces (−1.70 and −1.71 eV for ENL; −1.64 and −1.66 eV for MeA). Step edge and kink sites lower the adsorption energies by 0.4–0.5 eV compared to the terrace sites.

3.1.2. C–O bond dissociation products

MA has three different C–O bonds, i.e. the carbonyl C=O bond, the acetate-methyl (RCOO-R′) bond, and the acetyl–methoxy (RCO–OR′) bond. Acetate, acetyl, methoxy, formaldehyde are some of the products of the dissociation of these bonds in MA, ENL, and MeA, and CO may be a final product after complete decomposition of MA. Previously we calculated the lowest adsorption energies of these five species to be −2.23, −2.17, −1.84, −0.57, and −2.14 eV on Pd(1 1 1) [33], in close agreement with existing DFT studies (acetate: −2.28 eV [71]; acetyl: −2.01∼−2.20 eV [36,71]; methoxy: −1.68 to −1.73 eV [72,73]; formaldehyde: −0.45 to −0.54 eV [73,74]; CO: −1.80 to −2.14 eV [72,73,75,76]). Acetate, acetyl, methoxy, and CO are the likely major surface intermediates in this and related reaction systems [31,77,78]. Overall, of the molecular species in Table 1, either acetate or acetyl is the strongest adsorbing species on all the Pd surfaces, whereas formaldehyde and MA, which have closed-shell electronic configurations, are always the weakest adsorbing species.

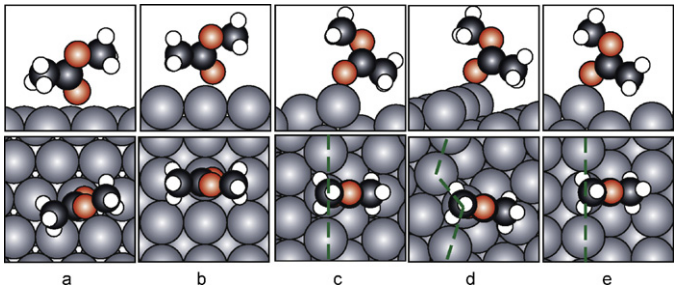

Fig. 2. The adsorption energy and geometry of MA on Pd surfaces: (a) Pd(1 1 1), (b) Pd(1 0 0), (c) Pd(6 6 3), (d) Pd(5 6 3), and (e) Pd(7 1 1). The top panels are side views and the bottom panels are top views. Large grey spheres = Pd; medium dark spheres = C; medium gray (red in the web version of the article) spheres = O; small white spheres = H. Same keys below.

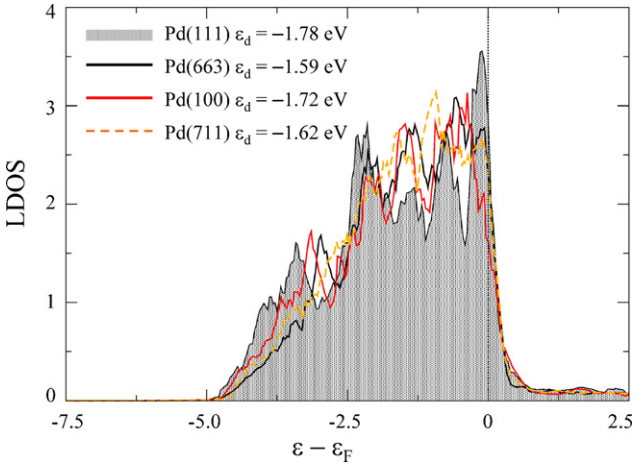

Fig. 3. Local density of d states (LDOS) projected onto surface Pd atoms on Pd(1 1 1), (6 6 3), (1 0 0), and (7 1 1) surfaces. ε_F denotes the energy of the Fermi level. The center of the *filled* d band (ε_d) is indicated in the legend. For brevity, the LDOS of Pd(5 6 3) is not included; its ε_d is −1.44 eV at the kink; −1.71 eV at the corner; and −1.54 eV along the step edge. The ε_d of Pd(1 1 1) was previously reported to be −1.8 eV [76,79].

Acetate always prefers a μ-O,O state occupying two Pd atoms. Acetyl adsorbs through the unsaturated C in η^1 (atop one Pd atom) and η^2 (bridging two Pd atoms) configurations that are nearly isoenergetic. Formaldehyde always adsorbs through the unsaturated C atop one Pd atom and through O either atop another Pd atom or bridging two adjacent Pd atoms. Both acetyl and formaldehyde prefer to align its C–O bond with the step edge in μ-C,O configurations on Pd(6 6 3) and (7 1 1). Methoxy prefers bonding through O in an fcc site on Pd(1 1 1) or bridging two Pd atoms at step edges and on Pd(1 0 0). Unlike the others, CO adsorbs most strongly on Pd(1 1 1) and least strongly on Pd(1 0 0).

Overall, the adsorption energies of these molecular species are affected by less than ±−0.1 eV from (1 1 1)- to the corresponding (1 0 0)-type surfaces. On the other hand, adsorption is clearly strengthened from terrace to step edge sites, with the effect being more pronounced for the (1 1 1)-type surfaces. This pattern closely mirrors how the center of Pd surface d band (ε_d) varies from one surface to another (see Fig. 3 for plots of the Pd d bands and associated ε_d): The ε_d up-shifts slightly from (1 1 1) to (1 0 0) terraces and down-shifts slightly from (1 1 1) to (1 0 0) step edges (by 0.06 and 0.03 eV, respectively), but from terrace to step edge of the same surface type the ε_d always up-shifts, particularly for the (1 1 1)-type surfaces (by 0.19 eV).

3.1.3. Atomic species

Atomic H, C, and O are likely to be present on Pd surfaces following the decomposition of the reactants in MA hydrogenolysis. Previous DFT studies reported the adsorption energies to be −2.66 to −2.84 eV for H [71,73,74,80], −6.21 to −6.65 eV for C [36,72], and −3.89 to −4.35 eV for O [72,81], whereas our previous results are slightly lower because of the 1/9 ML coverage employed in our study (−2.96, −7.12, and −4.46 eV on Pd(1 1 1)) [33].

The effect of surface structure on H, C, and O adsorption is different in the top and the hollow sites. In the top site, the adsorption

Table 1
Adsorption configurations and corresponding adsorption energies of various species on the Pd surfaces (E_{ads}; in eV); differences in adsorption energies between different Pd surfaces (Δ; in eV); and estimated diffusion barriers for the atomic species (E_d; in eV).

	Pd(1 1 1)		Pd(6 6 3)		Pd(5 6 3)		Pd(1 0 0)		Pd(7 1 1)		$\Delta((1\,1\,1)\rightarrow(1\,0\,0))$		Δ(terrace → step)		Δ(step → kink)
	Config.	E_{ads}	Config.	E_{ads}	Config.	E_{ads}	Config.	E_{ads}	Config.	E_{ads}	Terrace	Step	(1 1 1)	(1 0 0)	(1 1 1)
MA	O(t) (cis)	−0.21	O(t1) (cis)	−0.52	O(tk) (cis)	−0.51	O(t) (cis)	−0.22	O(t1) (cis)	−0.49	−0.01	+0.03	−0.31	−0.27	+0.01
ENL	H_2C(t)	−1.70	H_2C(t1)	−2.22	H_2C(t1)	−2.10	H_2C(t)	−1.71	H_2C(t1)	−2.12	−0.01	+0.10	−0.52	−0.41	+0.12
MeA	H_2C(t)	−1.64	H_2C(t1)	−2.11	H_2C(t1)	−2.07	H_2C(t)	−1.66	H_2C(t1)	−2.02	−0.02	+0.09	−0.47	−0.36	+0.04
Acetate	μ-O,O	−2.23	μ-O,O	−2.77	μ-O,O	−2.63	μ-O,O	−2.27	μ-O,O	−2.68	−0.04	+0.09	−0.54	−0.41	+0.14
Acetyl	C(t/b)–O(t)	−2.17	C(t1)–O(t1)	−2.45	C(t1)–O(tk)	−2.41	C(b)–O(b)	−2.32	C(t1)–O(t1)	−2.40	−0.15	+0.05	−0.28	−0.08	+0.04
Ketene	m-C,C	−1.19	C(t1)–C(t1)	−1.46	C(t1)–C(tk)	−1.44	C(t)–C(t)	−1.21	C(t1)–C(t1)	−1.42	−0.02	+0.04	−0.27	−0.21	+0.02
Methoxy	O(fcc) (upright)	−1.84	O(b1) (tilted)	−2.18	O(bck) (tilted)	−2.16	O(b) (upright)	−1.93	O(b1) (tilted)	−2.15	−0.09	+0.03	−0.34	−0.22	+0.02
Formaldehyde	C(t)–O(b)	−0.57	C(t1)–O(t1)	−0.91	C(t1)–O(tk)	−0.95	O(t)–C(t)	−0.63	C(t1)–O(t1)	−0.89	−0.06	+0.02	−0.34	−0.26	−0.04
CO	C(fcc)	−2.14	C(f1)	−2.13	C(f1)	−2.13	C(b)	−1.91	C(b1)	−2.06	+0.23	+0.07	+0.01	−0.15	0.00
H	t	−2.32	t1	−2.29	tk	−2.14	t	−2.25	t1	−2.26	+0.07	+0.03	+0.03	−0.01	+0.15 (top)
	b	*−2.81*	b1	*−2.76*	bck	−2.75	b	−2.72	hw1	−2.73					
	hcp	−2.83	f1	−2.88	f1	−2.87	hw	−2.75	b1	−2.77					
	fcc	−2.96	h2	−2.79	h2	−2.81			b12	−2.70	+0.21	+0.11	+0.08	−0.02	+0.01 (hollow)
			h3	−2.78	fk1	−2.71			h3	−2.77					
			f4	−2.68	hk2	−2.76			h4	−2.69					
	E_d(fcc → b)	0.15	E_d(f1 → b1)	0.12	E_d(f1 → bck)	0.12	E_d(hw → b)	0.03	E_d(hw1 → b12)	0.03					
C	t	−4.41	t1	−4.51	tk	−4.47	t	−4.40	t1	−4.50	+0.01	+0.01	−0.10	−0.10	+0.04 (top)
	b	*−6.29*	b1	−6.27	bck	*−5.89*	b	*−5.99*	hw1	−7.86					
	hcp	−7.12	f1	−7.00	f1	−6.99	hw	−7.88	b1	−6.24					
	fcc	−6.85	h2	−7.00	h2	−7.19			b12	−6.04	−0.76	−0.86	+0.12	+0.02	−0.19 (hollow)
			h3	−6.84	fk1	−7.53			h3	−6.96					
			f4	−7.42	hk2	−6.79			h4	−6.68					
					hwk3	−7.66									
	E_d(hcp → b)	0.83	E_d(f1 → b1)	0.73	E_d(h2 → bck)	1.30	E_d(hw → b)	1.89	E_d(hw1 → b12)	1.82					
O	t	−2.81	t1	−3.17	tk	−3.13	t	−2.89	t1	−3.15	−0.08	+0.02	−0.36	−0.26	+0.04 (top)
	b	*−3.96*	b1	−4.12	bck	−4.09	b	−3.85	hw1	−4.16					
	hcp	−4.14	f1	−4.40	f1	−4.34	hw	−4.16	b1	−4.22	+0.30	+0.18	+0.06	−0.06	+0.06 (hollow)
	fcc	−4.46	h2	−4.11	h2	−4.21			b12	−3.93					
			h3	−4.08	fk1	−3.89			h3	−4.14					
			f4	−3.60	hk2	−4.00			h4	−3.90					
	E_d(fcc → b)	0.50	E_d(f1 → b1)	0.28	E_d(h2 → bck)	0.12	E_d(hw → b)	0.31	E_d(hw1 → b12)	0.23					

See Fig. 1 for site designations. Multiple high symmetry states are included for atomic species, whereas only the preferred states are listed for molecular species. Representative diffusion pathways for atomic species are indicated. Italicized configurations are calculated by constraining the atom in place. For C on Pd(6 6 3) and (5 6 3), the differences (Δ) are calculated using the underlined values.

energies of all three species change by less than 0.1 eV from (1 1 1)- to the corresponding (1 0 0)-type surfaces. On the other hand, from terrace to step edge of the same surface type, while H adsorption is barely affected [49], the adsorption of C and O is strengthened. This pattern also holds for the molecular species, which makes sense since most of them bond through C or O to the top of a Pd atom, and since it reflects the positions of the local d-band centers.

A different pattern is seen for adsorption in the (1 1 1)-type threefold and (1 0 0)-type fourfold hollow sites: From (1 1 1)- to the corresponding (1 0 0)-type surfaces, where the number of Pd neighbors increases in the hollow sites, the adsorption of H and O is destabilized while that of C is substantially stabilized. On the other hand, from hollow sites in terraces to those along step edges, where the number of Pd neighbors does not change, the adsorption of none of the three species is affected much. This does not reflect the positions of the local d-band centers but rather suggests that the adsorption of the atomic species responds strongly to the coupling to the neighboring Pd atoms in the hollow sites. The strong stabilization of C in the fourfold hollow sites compared to the threefold hollow sites reflects the need of the C atom to satisfy its valence. Conversely, for H and O whose valance is already saturated in the threefold sites, greater overlap with Pd states in the fourfold sites produces a repulsive interaction instead.

The mono-atomic steps of Pd(6 6 3) and (5 6 3) expose fourfold hollow-like sites (f4 in Fig. 1b; hwk3 in Fig. 1c), in which C adsorbs more strongly than any other site along these step edges. Therefore, C should preferentially occupy the lower side of the Pd(6 6 3) and (5 6 3) step edges, whereas H and O prefer the upper-edge sites instead. The sites on the lower side of the (7 1 1) step edge (h3 and f4 in Fig. 1d) do not have fourfold square geometry and so do not bind C more strongly than the upper terrace does. When an edge is multi-atomic high or is formed by two extended terraces, the lower edge sites will not be present.

By assuming two-fold bridge sites to be the local maxima between adjacent hollow sites, we can also estimate the diffusion barrier required for the atomic species to diffuse from the more stable adsorption sites on each surface (Table 1). For H the diffusion barrier is 0.15 eV and less on all the Pd surfaces included in this study. For O, the highest of the diffusion barriers is 0.50 eV on (1 1 1) terrace. For C, the diffusion barrier is ca. 0.8 eV on (1 1 1)-type surfaces and 1.8 eV on (1 0 0)-type surfaces. Therefore, H and O atoms are mobile across Pd surfaces at typical hydrogenolysis reaction temperature, whereas C atoms diffuse much more slowly and will poison (1 0 0)-type surfaces in particular, if they are generated and not reacted away.

3.2. Pd(1 1 1)

The activation of MA on the close-packed Pd(1 1 1) terrace has been reported by us previously [33] and will only be summarized here (Fig. 4). MA interacts weakly with Pd(1 1 1) ($E_{ads} = -0.21$ eV; Fig. 2), so its C–O bonds remain strong: The dissociation barrier is 1.00 eV for the acetyl–methoxy bond and significantly higher for the acetate-methyl ($E_a = 1.92$ eV) and carbonyl ($E_a = 2.31$ eV) bonds. Dehydrogenation, on the other hand, has lower barriers ($E_a = 0.74$ eV yielding ENL; 0.82 eV yielding MeA). In ENL and MeA, C–O bond dissociation occurs most readily also in the RCO–OR′ position ($E_a = 1.10$ eV in ENL and 0.61 eV in MeA), whereas dehydrogenation occurs most readily at the unsaturated C center ($E_a = 0.81$ eV in ENL and 0.83 eV in MeA). The calculated and estimated reaction barriers suggest that the most facile reaction pathway for MA on clean Pd(1 1 1) is successive dehydrogenation at the acetate end leading to non-selective decomposition, and the apparent E_a with respect to gas-phase MA (0.74 − 0.21 = 0.53 eV) is sufficiently low to permit substantial rates at moderate temperatures, in qualitative agreement with available experimental evidence [11,13,31].

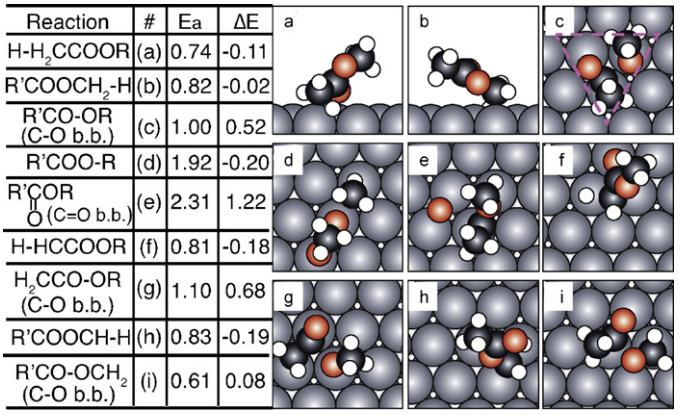

Fig. 4. C–H and C–O bond dissociation steps in MA (a–e), ENL (f–g), and MeA (h–i) on Pd(1 1 1). The dissociating bond is indicated by a hyphen. The table on the left lists the activation barrier (E_a) and reaction energy (ΔE) of each step relative to the adsorbed reactant. The panels on the right show the top view of the TS of each step (except (a) and (b) showing side views). See Section 3.6 for purpose of the dashed triangle in (c).

We also note that both C–H and C–O bond dissociation requires an ensemble of at least two adjacent Pd atoms, but while C–H bonds dissociate over the top of a single Pd atom being constrained by the short C–H bond length, the RCO–OR′ bonds dissociate over a bridge site and involves no sharing of Pd atoms.

3.3. Pd(6 6 3)

Pd(6 6 3) is used to represent the step edge of a Pd(1 1 1) terrace. The activation barriers for dehydrogenation at both ends of MA are lowered when it occurs along the step edge (on the t1 site; $E_a = 0.52$ and 0.68 eV; Fig. 5a, 5b) than on the (1 1 1) terrace ($E_a = 0.74$

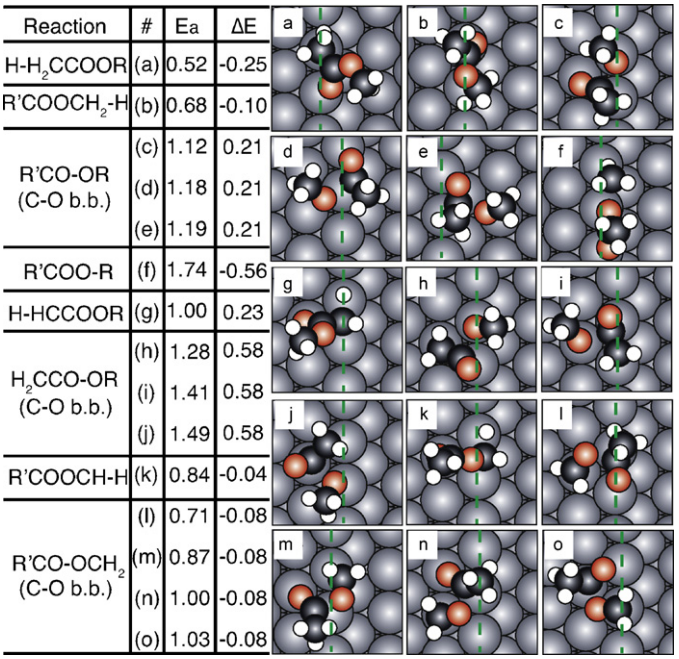

Fig. 5. C–H and C–O bond dissociation steps in MA (a–f), ENL (g–j), and MeA (k–o) on Pd(6 6 3) step edge. The dissociating bond is indicated by a hyphen. The table on the left lists the activation barrier (E_a) and reaction energy (ΔE) of each step. The panels on the right show the top view of the TS of each step.

and 0.82 eV [33]). Because of the reduced symmetry of the surface, multiple channels are explored for dissociating the acetyl–methoxy bond in MA, including dissociation along the step edge (Fig. 5c), perpendicular to the edge (Fig. 5d), and against the edge (Fig. 5e). The activation barriers for the three channels are 1.12, 1.18, and 1.19 eV respectively. While there is no sharing of Pd atoms in the TS of the C–O bond dissociation step, the short lengths of C–H bonds cause the dissociating C and the H always to share a Pd atom. Consequently, dissociating against the step edge (e.g. Fig. 5e) offers no advantage to either type of process. This is different from the dissociation of diatomic molecules which can be substantially promoted by occurring against step edges to avoid sharing of metal atoms as occurs on the close-packed terraces [41,48,51,53]. Any enhancement of C–O and C–H bond dissociation in MA at the step edge is therefore due primarily to the altered electronic structures of the step edge Pd atoms. The methyl-acetate bond remains very strong (E_a = 1.74 eV; Fig. 5f) because, like Pd(1 1 1), the step edge cannot effectively stabilize the TS of its dissociation. We will therefore ignore the dissociation of the methyl-acetate and carbonyl C–O bonds and refer only to the RCO–OR′ bond when discussing C–O bond dissociation henceforth.

The dehydrogenation of ENL and MeA involves the unsaturated C center, which moves to a bridge site along the step edge (b1 site) to satisfy its fourfold valence, with the dissociating H atom located on the adjacent t1 top site. The barriers are 1.00 and 0.84 eV, respectively. Like on Pd(1 1 1), breaking the RCO–OR′ bond is easier in MeA than in MA. Several reaction channels are investigated (Fig. 5l–o), with the lowest barrier being 0.71 eV.

A comparison of the activation barriers (Fig. 5) with those on Pd(1 1 1) (Fig. 4) shows that some of the activation barriers on Pd(6 6 3) are slightly higher than the corresponding ones on Pd(1 1 1). This is because the adsorption of the adsorbed reactants (MA, ENL, and MeA) is enhanced by 0.3–0.5 eV from Pd(1 1 1) to Pd(6 6 3), outstripping the stabilization of some of the TSs. However, the lowest-energy TS of every step on Pd(6 6 3) is stabilized compared to that of the same step on Pd(1 1 1), indicating that the apparent E_a, as relative not to adsorbed MA but to gas-phase MA, will all be lower at the step edge.

3.4. Pd(5 6 3)

The Pd(5 6 3) surface features a kink at the edge of the terrace. The d band center (ε_d) at the kink is up-shifted (Fig. 3) compared to the Pd(6 6 3) step edge because the kink atom has one fewer neighbor than the step edge atoms (Fig. 1). However, the effect of this under-coordination is quite local: Just one atom over along the step edge, the ε_d is already approaching that of the continuous step edge, and for a one-atom-wide kink like Pd(5 6 3), the kink is immediately abutted on the other side by a corner where a Pd atom is missing only one neighbor compared to the (1 1 1) terrace. The effect of the kink atom on reactivity is indeed limited, as is reflected in the lack of any significantly change in the adsorption energies compared to Pd(6 6 3) (Table 1). The nearly identical adsorption energies in turn translate into a lack of change in the barriers of bond dissociation that occurs at and around the kink site. Because of the reduced surface symmetry, we have also checked multiple reaction channels for each bond dissociation step for MA (Fig. 6). The lowest activation barriers for C–H bond and RCO–OR′ C–O bond dissociation are nearly identical to those on the Pd(6 6 3) step edge (cf. Fig. 5a–c), with the formation of ENL being the most facile process as before (E_a = 0.53 eV; Fig. 6a). The same elementary steps occurring in alternate sites around the kink have similar activation barriers. We conclude that the kink atom does not clearly promote bond dissociation compared to the step edge because it is the only one with an up-shifted ε_d, whereas more than one Pd atom is needed to stabilize the TSs. The similar reactivities of Pd step edge and kink have been noted for CH_4 and CO dissociation, with which our findings are in agreement [49].

Reaction	#	Ea	ΔE
H-H_2CCOOR	(a)	0.53	-0.17
	(b)	0.64	-0.17
	(c)	0.71	-0.17
R'$COOCH_2$-H	(d)	0.72	-0.11
	(e)	0.75	-0.11
	(f)	0.84	-0.11
	(g)	0.95	-0.11
R'CO-OR (C-O b.b.)	(h)	1.10	0.28
	(i)	1.10	0.28
	(j)	1.12	0.28
	(k)	1.17	0.28
	(l)	1.19	0.28
R'COO-R	(m)	1.93	-0.42

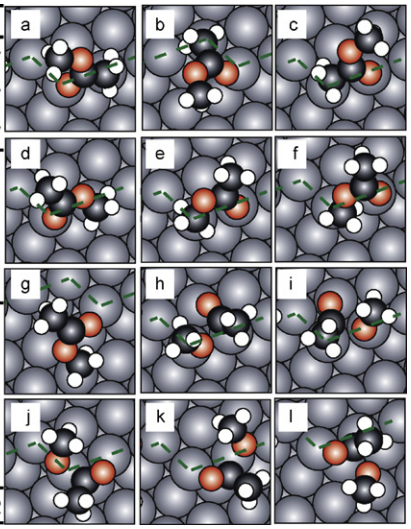

Fig. 6. C–H and C–O bond dissociation steps in MA on kinked Pd(5 6 3). The dissociating bond is indicated by a hyphen. The table on the left lists the activation barrier (E_a) and reaction energy (ΔE) of each step. The panels on the right show the top view of the TS of each step (except (m)).

3.5. Pd(1 0 0) and Pd(7 1 1)

The TSs of the C–H and C–O bond dissociation steps on Pd(1 0 0) resemble those on Pd(1 1 1), and the activation barriers for dehydrogenation are nearly identical on the two surfaces 0.71 eV for ENL formation and 0.84 eV for MeA formation (Fig. 7a and b), vs. 0.74 and 0.82 eV, respectively, on Pd(1 1 1) (Fig. 4a and b). However, the activation barrier for dissociating the acetyl–methoxy bond is clearly lower than on Pd(1 1 1) (0.84 eV (Fig. 7c) vs. 1.00 eV). Likewise, for ENL and MeA, the activation barriers for C–O bond dissociation are lowered more than the barriers for C–H bond dissociation are, from Pd(1 1 1) to Pd(1 0 0): The activation barriers for dissociating the RCO–OR′ bond are 1.10 and 0.61 eV on Pd(1 1 1) and 0.92 and 0.31 eV on Pd(1 0 0), for ENL and MeA respectively. On the other hand, dehydrogenating the unsaturated C center in ENL and MeA need to overcome activation barriers of 0.81 and 0.83 eV on Pd(1 1 1) and 0.73 and 0.66 eV on Pd(1 0 0), respectively.

Reaction	#	Ea	ΔE
H-H_2CCOOR	(a)	0.71	0.08
R'$COOCH_2$-H	(b)	0.84	0.16
R'CO-OR (C-O b.b.)	(c)	0.84	0.29
R'COO-R	(d)	1.79	-0.20
H-HCCOOR	(e)	0.73	0.04
H_2CCO-OR (C-O b.b.)	(f)	0.92	0.57
R'COOCH-H	(g)	0.66	-0.00
R'CO-OCH_2 (C-O b.b.)	(h)	0.31	-0.11
R'COO-CH_2 (C-O b.b.)	(i)	0.88	-0.31

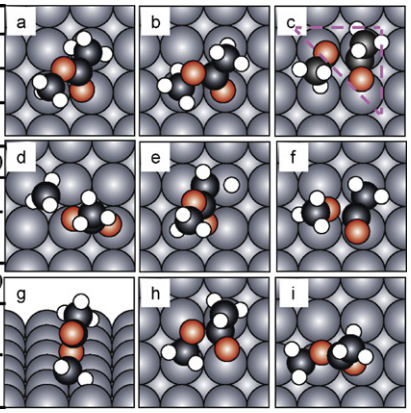

Fig. 7. C–H and C–O bond dissociation steps in MA (a–d), ENL (e–f), and MeA (g–i) on Pd(1 0 0). The dissociating bond is indicated by a hyphen. The table on the left lists the activation barrier (E_a) and reaction energy (ΔE) of each step. The panels on the right show the top view of the TS of each step (except (g) which shows a rotated side view). See Section 3.6 for purpose of the dashed triangle in (c).

Reaction	#	Ea	ΔE
H-H_2CCOOR	(a)	0.75	-0.06
R'COOCH_2-H	(b)	0.91	0.06
R'CO-OR (C-O b.b.)	(c)	0.93	0.34
	(d)	0.98	0.34
	(e)	1.00	0.34
	(f)	1.06	0.34
H-HCCOOR	(g)	0.92	0.23
H_2CCO-OR (C-O b.b.)	(h)	1.15	0.53
	(i)	1.24	0.53
	(j)	1.28	0.53
R'COOCH-H	(k)	0.74	0.04
R'CO-OCH_2 (C-O b.b.)	(l)	0.48	0.00
	(m)	0.51	0.00
	(n)	0.61	0.00
	(o)	0.69	0.00

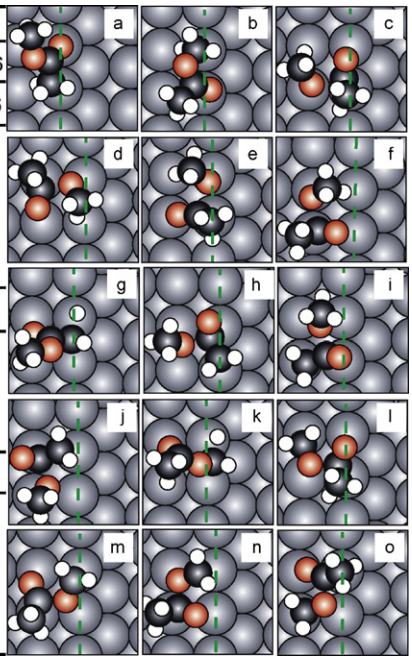

Fig. 8. C–O and C–H bond dissociation steps in MA (a–f), ENL (g–j), and MeA (k–o) on Pd(7 1 1) step edge. The dissociating bond is indicated by a hyphen. The table on the left lists the activation barrier (E_a) and reaction energy (ΔE) of each step. The panels on the right show the top view of the TS of each step.

The same trend pattern extends to Pd(7 1 1), which represents the step edge of a (1 0 0) terrace. In MA the barrier for directly activating the acetyl–methoxy C–O bond is also nearly identical to that of C–H bond dissociation forming MeA (Fig. 8b and c). The activation barriers for MA at Pd(7 1 1) step edge are slightly higher than those on Pd(1 0 0), which masks the fact that the TSs are in fact stabilized, but not as much as the reactant (MA) is by the step edge, similar to what is seen at the Pd(6 6 3) step edge when compared to Pd(1 1 1).

3.6. Comparison of C–O bond dissociation on different Pd surface structures

Overall, therefore, the dissociation of the ester RCO–OR′ C–O bond is more promoted than C–H bond dissociation from the (1 1 1)- to (1 0 0)-type surfaces, and so the rate constant for cleaving the C–O bond to generate the acetyl species should be higher on the latter. The differential promotion cannot be explained by the position of the surface d-band center or the adsorption energies of atomic C and O in the top site, but has to do with the different arrangements of the surface atoms. We compare the geometries of the TSs of the lowest-barrier C–O bond dissociation steps in MA, ENL, and MeA on the different Pd surfaces in Table 2. A possible factor stabilizing the C–O bond dissociation TSs on the (1 0 0)-type surfaces is the wider O–C–O bond angle than on the (1 1 1)-type surfaces. The molecularly adsorbed MA on Pd(1 1 1) and (1 0 0) (Fig. 2a and b) has an O–C–O bond angle of 121°, which is indicative of sp2 hybridization of the central C. In the TS, however, the central C is involved in bonding interactions with four atoms simultaneously: the Pd atom on which it is situated, the methyl C atom, and the two O atoms, which requires the central C to be briefly sp3-hybridizd, and it takes a triangular ensemble of Pd atoms to stabilize the TS. On Pd(1 1 1) such an ensemble of Pd atoms form an isosceles triangle (illustrated by dashed lines in Fig. 4c), whereas on Pd(1 0 0) they form a right triangle (illustrated by dashed lines in Fig. 7c).

Table 2
Geometric parameters of the RCO–OR′ bond dissociation in MA, ENL, and MeA on the fixed Pd surfaces, including the length of the dissociating C–O bond (d(C–O), in Å) and the angle formed by the carbonyl O, the central C, and the dissociating O atoms (∠(O–C–O), in°).

Surfaces	MA		ENL		MeA	
	d(C–O)	∠(O–C–O)	d(C–O)	∠(O–C–O)	d(C–O)	∠(O–C–O)
Pd(1 1 1)	2.13 (4c)	101.3	1.97 (4g)	107.7	2.16 (4i)	106.1
Pd(6 6 3)	2.10 (5c)	103.2	2.00 (5l)	108.9	2.23 (5h)	104.9
Pd(1 0 0)	2.15 (7c)	105.1	1.80 (7h)	108.9	1.93 (7f)	110.1
Pd(7 1 1)	2.13 (8c)	107.7	1.82 (8h)	109.6	1.98 (8l)	109.7

The labels in the parentheses following d(C–O) values indicate which figure and panel depict the TSs.

A typical sp3-hybridized C with four identical bonds should have each bond angle at 109°. The square geometry of the (1 0 0) surface evidently provides a less constraining site than the hexagonal geometry of the (1 1 1) surface, allowing the O–C–O bond angle to approach the optimal value of 109°. On the other hand, C–H bond dissociation steps always occur over a single Pd atom with C and H constrained to sharing a Pd atom by the short C–H bond length, and are therefore insensitive to the different arrangements of the surface atoms (Fig. 9).

Having calculated a number of different C–H (including both saturated and unsaturated C centers) and C–O bond dissociation steps in MA, ENL, and MeA, we can also gain a measure of the surface structural effect on C–H and C–O bond dissociation activity by comparing the corresponding TS energies (E_{TS}; with respect to the reactant in gas phase) on (1 0 0)- and (1 1 1)-type surfaces; and step edges with terraces of the same surface type (Table 3). Comparison of the E_{TS} on different surfaces can reveal the effect of the surface structure on selectivity if it is done for steps issuing from the same reactant.

For instance, from (1 1 1) to (1 0 0) terrace sites, the E_{TS} of dissociating the C–H bonds in MA barely changes (by −0.03 and +0.01 eV for forming ENL and MeA), but the TS of acetyl–methoxy bond dissociation in MA is stabilized by 0.17 eV. That is, the TS of acetyl–methoxy bond dissociation is 0.14 eV more stable relative to the TS of C–H bond dissociation (forming ENL) on (1 0 0) terrace than on (1 1 1) terrace. The stabilization of the TSs of the RCO–OR′ bond dissociation by (1 0 0)-type surfaces relative to those of C–H bond dissociation holds true for MA, ENL, and MeA, on both terrace and edge sites. It is due as much to the stabilization of the TSs of the C–O bond dissociation as to a lack of stabilization of the TSs of the C–H bond dissociation.

If we compare the E_{TS} in a different way, i.e. between the terrace and step edge sites of the same surface type, the results are quite different. For instance, from (1 1 1)-type terrace to step edge, while the TS of C–O bond dissociation in MA is stabilized by 0.20 eV, the TSs of C–H bond dissociation are stabilized by 0.54 and 0.46 eV, respectively. The same differential stabilization holds true from (1 0 0)-type terrace to step edge, albeit to a less extent.

Table 4 summarizes the comparisons by averaging the changes in the E_{TS} listed in Table 3, showing that C–H and C–O bond dissociation in MA and its derivatives are indeed preferentially promoted by step edges and (1 0 0) terraces, respectively, relative to Pd(1 1 1). Earlier studies have suggested that substantial dehydrogenation facilitates undesirable C–C bond dissociation [21,34–36]. Here we suggest that the surface structural effect is such that, to increase the selectivity for ethanol, at least in terms of how MA is activated, it would be best to disable step edges but increase the concentration of Pd(1 0 0) facets relative to Pd(1 1 1) facets. It should be noted that the dehydrogenation of MA, especially via the successive dehydrogenation of ENL [33], is a major pathway in competition with the dissociation of the C–O bond in MA and will therefore limit the selectivity for alcohol on all these Pd surfaces.

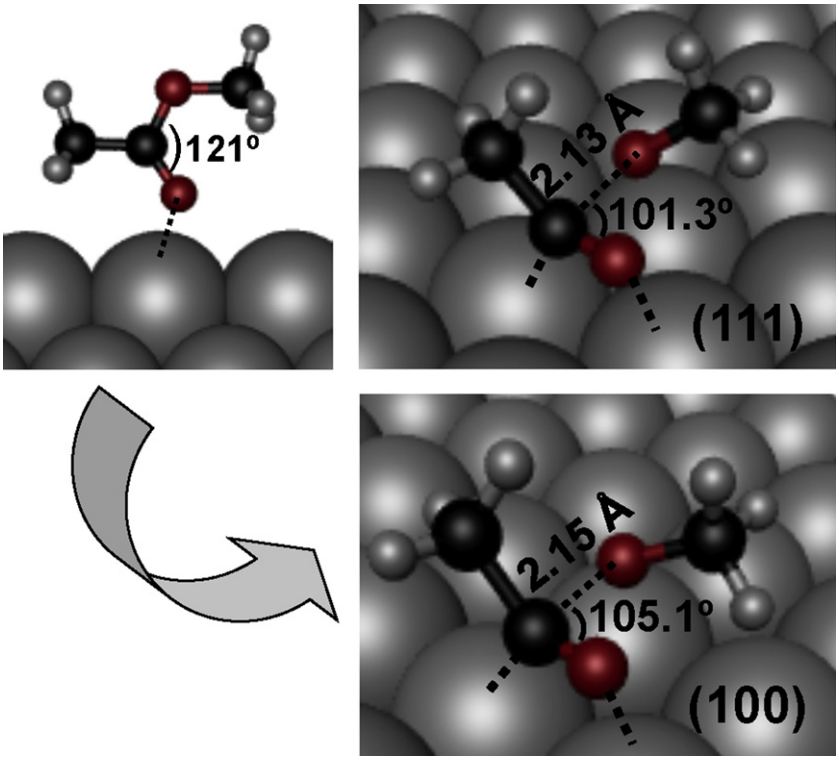

Fig. 9. Evolution of the geometry of MA in the dissociation of the RCO–OR′ bond. The ∠(O–C–O) bond angle and d(C–O) bond distance are labeled. The panel on the left shows molecularly adsorbed MA, which has identical ∠(O–C–O) bond angles on Pd(1 1 1) and (1 0 0). The top and bottom panels on the right show the TSs on Pd(1 1 1) and (1 0 0) as described in Figs. 4c and 7c, respectively. Dashed lines signify formal bonds. Large grey spheres = Pd; medium dark spheres = C; medium gray (red) spheres = O; small white spheres = H.

To assess the effect of surface relaxation, we have repeated the calculations for the lowest-energy C–H and C–O bond dissociation TSs on relaxed surfaces and show the differences in E_{TS} on the relaxed surfaces in Table 5, with the averaged values already included in Table 4. It can be seen that surface relaxation does not change the conclusions regarding the selectivity between C–H and C–O bond dissociations, indicating that the structural effect on the selectivity is intrinsic to the geometric and electronic properties of the different Pd surfaces.

Our conclusions about the structural effect on the selectivity of MA activation on Pd need to be verified experimentally or through detailed kinetic modeling taking into account of the coverages of various surface species.

3.7. Linear energy relations for C–H and C–O bond dissociation

In line with previous reports [21,33,35,82,83], the large number of C–H and C–O bond dissociation steps investigated in this study form Brønsted–Evans–Polanyi (BEP) type linear energy relations between E_{TS} and E_{FS} (Fig. 10). For all the C–H bond dissociation steps, linear regression finds $E_{TS} = 0.986\,E_{FS} + 0.760$ eV ($R^2 = 0.986$). For all the C–O bond dissociation (RCO–OR′ position) steps, linear regression finds $E_{TS} = 1.037\,E_{FS} + 0.636$ eV ($R^2 = 0.963$). The near-unity slopes are consistent with previously reported BEP relations for C–H and C–O bond dissociations in small oxygenates on Pd and other metals [21,33–36], which suggest that the two dissociating fragments in each of these bond-breaking TSs resemble the individual products structurally, i.e. the TSs are FS-like to nearly the same extent, thus causing the E_{TS} to vary in sync with E_{FS}. It

Table 4
The average of the differences in E_{TS} (in eV) as tabulated in Tables 3 (fixed surface) and 5 (relaxed surface).

	Fixed	Relaxed
Δ((1 1 1) → (1 0 0)), including terrace and step edge		
C–H	0.03	−0.01
C–O	−0.17	−0.21
Δ(terrace → step), including (1 1 1) and (1 0 0) surfaces		
C–H	−0.34	−0.27
C–O	−0.25	−0.17

Table 3
Differences in E_{TS} (in eV) for C–H and C–O (RCO–OR′ position) bond dissociation steps for MA, ENL, and MeA between (1 1 1)- and (1 0 0)-type surfaces, and between terrace and step edge sites.

	MA →			ENL →		MeA →	
	ENL + H	MeA + H	Acetyl + methoxy	$CHCOOCH_3$ + H	Ketene + methoxy	CH_3COOCH + H	Acetyl + formaldehyde
Δ((1 1 1) → (1 0 0))							
Terrace	−0.03	+0.01	−0.17	−0.08	−0.20	−0.21	−0.32
Step	+0.27	+0.27	−0.16	+0.02	−0.02	−0.02	−0.16
Δ(terrace → step)							
(1 1 1)	−0.54	−0.46	−0.20	−0.31	−0.34	−0.48	−0.37
(1 0 0)	−0.24	−0.20	−0.19	−0.21	−0.17	−0.29	−0.20

The lowest-energy TS of each step on each surface as shown in Figs. 4–8 are used in the comparisons.

Table 5
Differences in E_{TS} (in eV) on relaxed surfaces for C–H and C–O (RCO–OR′ position) bond dissociation steps for MA, ENL, and MeA between (1 1 1)- and (1 0 0)-type surfaces, and between terrace and step edge sites.

	MA →			ENL →		MeA →	
	ENL + H	MeA + H	Acetyl + methoxy	$CHCOOCH_3$ + H	ketene + methoxy	CH_3COOCH + H	Acetyl + formaldehyde
Δ((1 1 1)→(1 0 0))							
Terrace	−0.06	+0.01	−0.15	−0.07	−0.17	−0.12	−0.30
Step	+0.19	+0.20	−0.17	−0.08	−0.25	−0.11	−0.21
Δ(terrace → step)							
(1 1 1)	−0.45	−0.37	−0.15	−0.19	−0.08	−0.28	−0.27
(1 0 0)	−0.20	−0.18	−0.18	−0.20	−0.15	−0.27	−0.18

The lowest-energy TS of each step on each surface as shown in Figs. 4–8 are re-calculated on relaxed slabs and used in the comparisons.

is also worthwhile to point out that the FSs involving more saturated C centers tend to lie higher on each line and vice versa [33], which suggests that the dissociation of more saturated intermediates is more likely to be rate-controlling in the activation of MA.

The standard errors for the C–H and C–O relations are 0.089 and 0.181 eV respectively, the latter being of the same magnitude as the average differences in the E_{TS} due to structural effects (cf. Table 4). This indicates that the C–O relation, in particular, does not offer sufficient accuracy to allow the determination of selectivity between C–H and C–O bond dissociation for the intermediates in the reaction of MA or similar oxygenates. Standard errors on the order of 0.1 eV and greater have also been reported before for similar BEP relations [21,34–36]. Given that the selectivity of a reaction can be determined by differences of only a few tenths of an eV in activation barriers [54,84], the ability of these particular BEP relations to predict selectivity would appear to be limited by a lack of sufficient accuracy [35], although this should not reduce their utility in identifying rate-limiting steps and estimating reaction rates.

If we separate the C–O bond dissociation relation into one for the (1 1 1)-type surfaces and one for the (1 0 0)-type surfaces (see inset, Fig. 10), we obtain $E_{TS} = 1.000 \cdot E_{FS} + 0.669$ eV ($R^2 = 0.957$; standard error = 0.210 eV) for the former and $E_{TS} = 1.064\,E_{FS} + 0.586$ eV ($R^2 = 0.986$; standard error = 0.121 eV). Although the (1 1 1) relation is slightly less perfect than the (1 0 0) relation, they do not qualitatively change the conclusions above. These two BEP relations are similar owing to the similar geometries of the C–O bond dissociation TSs, in contrast to BEP relations for diatomic dissociation on close-packed and open surfaces, where the TS geometries are substantially different [48,85].

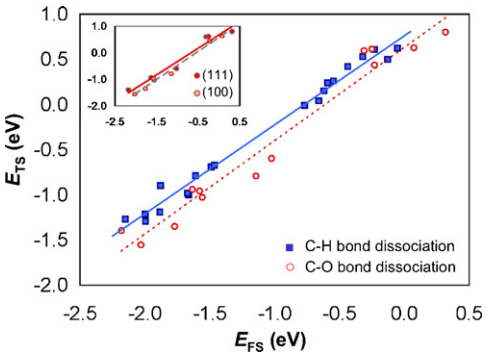

Fig. 10. Brønsted–Evans–Polanyi (BEP) relations for C–H (blue squares and solid line) and RCO–OR′ (red circles and dashed line) bond dissociation steps for MA, ENL, and MeA on the various Pd surfaces. The transition state energy (E_{TS}) and the final state energy (E_{FS}) are calculated relative to the corresponding reactant molecule in the gas phase, and can be directly calculated from the E_a and ΔE included in Figs. 4–8 and the adsorption energies of the respective reactants in Table 1. The inset separates the RCO–OR′ relation into one for (1 1 1)-type surfaces (red, solid line) and one for (1 0 0)-type surfaces (gray, dashed line).

4. Conclusions

Periodic DFT calculations have been performed to study the activation of methyl acetate (CH_3COOCH_3; MA) and its dehydrogenated derivatives, enolate (CH_2COOCH_3; ENL) and methylene acetate (CH_3COOCH_2; MeA), via C–H and C–O bond dissociation on (1 1 1)-type Pd terrace, step edge (Pd(6 6 3)), and kink (Pd(5 6 3)); and on (1 0 0)-type Pd terrace and step edge (Pd(7 1 1)).

The adsorption energies of MA, ENL, MeA, and several dissociation products (including acetate, acetyl, ketene, methoxy, formaldehyde, CO, C, O, and H) have been calculated. The adsorption of most of these species is nearly unaffected between (1 1 1)- and (1 0 0)-type surfaces, but is clearly enhanced by step edge vs. the corresponding terrace sites. Adsorption at the Pd(5 6 3) kink is indistinguishable from the continuous step edge of Pd(6 6 3). The adsorption energies of the molecular species, as well as the atomic species in the top sites, closely mirror the position of the local d-band center, with less coordinated Pd atoms possessing more up-shifted d-band centers and enhancing adsorption. On the other hand, atomic adsorption in the threefold and fourfold hollow sites does not correlate with the d-band centers, and instead reflects the extent of local coordination to neighboring Pd atoms and the intrinsic valence of the atomic species.

Strong promotion of bond dissociation on open surfaces and under-coordinated sites as is the case for diatomic molecules is not observed for MA and its derivatives. This is because the C–H bonds are constrained by the short bond lengths to dissociate over the top of a single Pd atom regardless of the surface structure, whereas the dissociation of the RCO–OR′ C–O bonds involves no sharing of Pd atoms, in the TS. The moderate promotion of C–O and C–H bond dissociation that we found is attributed to the different electronic structures of the step edge Pd atoms, and for C–O bond dissociation in particular, to the square symmetry of the (1 0 0) facet, which is geometrically less constraining than the hexagonal symmetry of the (1 1 1) facet for stabilizing the sp3-hybridized O–C–O center in the TSs.

By comparing the TS energies of the same C–H and C–O bond dissociation steps on the different Pd surfaces, we found that, among the terraces and step edges of the (1 1 1) and (1 0 0) facets of Pd, relative to the (1 1 1) terrace, the (1 0 0) terrace preferentially promotes C–O bond dissociation, whereas the step edges, especially the step edges of (1 1 1) terraces, preferentially promote C–H bond dissociation. We suggest that the surface structural effect is such that, to increase the selectivity for ethanol, it would be best to block Pd step edges but increase the concentration of Pd(1 0 0) facets relative to Pd(1 1 1) facets, as far as MA activation is concerned. Our findings may have general implications in the activation of C–O bonds in carboxylic esters and acids on the surfaces of Pd and other fcc metals [71,86].

While Brønsted–Evans–Polanyi type linear energy relations with excellent coefficients of correlation have been obtained for all the C–H and C–O bond dissociation steps in this study, the standard errors, particularly for C–O bond dissociation, are on the same

order of magnitude as the structural effect on TS energies, which would limit the ability of these BEP relations to predict reaction selectivity.

Acknowledgments

This work was financially supported by Eastman Chemical Company and performed at the Center for Nanophase Materials Science, which is sponsored at Oak Ridge National Laboratory (ORNL) by the Division of Scientific User Facilities, U.S. Department of Energy. Computing resources provided by the Texas Advanced Computing Center (TACC), the National Center for Computing Sciences (NCCS), and ORNL were used and are gratefully acknowledged.

References

[1] H. Adkins, K. Folke, J. Am. Chem. Soc. 53 (1931) 1095.
[2] H. Adkins, B. Wojcik, L.W. Covert, J. Am. Chem. Soc. 55 (1933) 1669.
[3] K. Folke, H. Adkins, J. Am. Chem. Soc. 54 (1932) 1145.
[4] T. Turek, D.L. Trimm, Catal. Rev. Sci. Eng. 36 (1994) 645.
[5] G.W. Huber, S. Iborra, A. Corma, Chem. Rev. 106 (2006) 4044.
[6] M. Snåre, I. Kubickova, P. Mäki-Arvela, K. Eränen, J. Warna, D.Y. Murzin, Chem. Eng. J. 134 (2006) 29.
[7] A. Corma, S. Iborra, A. Velty, Chem. Rev. 107 (2007) 2411.
[8] P.T. Do, M. Chiappero, L.L. Lobban, D.E. Resasco, Catal. Lett. 130 (2009) 9.
[9] J.W. Evans, M.S. Wainwright, N.W. Cant, D.L. Trimm, J. Catal. 88 (1984) 203.
[10] M.A. Kohler, N.W. Cant, M.S. Wainwright, D.L. Trimm, Proc. Int. Cong. Catal. 9 (1988) 1043.
[11] P. Claus, M. Lucas, B. Lucke, T. Berndt, P. Birke, Appl. Catal. A: Gen. 79 (1991) 1.
[12] O.A. Ferretti, J.P. Bournonville, G. Mabilon, G. Martino, J.P. Candy, J.M. Basset, J. Mol. Catal. 67 (1991) 283.
[13] P.S. Wehner, B.L. Gustafson, J. Catal. 135 (1992) 420.
[14] D.J. Thomas, J.T. Wehrli, M.S. Wainwright, D.L. Trimm, N.W. Cant, Appl. Catal. A: Gen. 86 (1992) 101.
[15] B.E. Green, C.S. Sass, L.T. Germinario, P.S. Wehner, B.L. Gustafson, J. Catal. 140 (1993) 406.
[16] T. Turek, D.L. Trimm, D.S. Black, N.W. Cant, Appl. Catal. A: Gen. 116 (1994) 137.
[17] D.S. Brands, E.K. Poels, A. Bliek, Appl. Catal. A: Gen. 184 (1999) 279.
[18] M.A. Natal Santiago, M.A. Sanchez-Castillo, R.D. Cortright, J.A. Dumesic, J. Catal. 193 (2000) 16.
[19] A.B. Sanchez, N. Homs, J.L.G. Fierro, P.R. de la Piscina, Catal. Today 107–08 (2005) 431.
[20] A. El Mansour, J.P. Candy, J.P. Bournonville, O.A. Ferretti, J.M. Basset, Angew. Chem. Int. Ed. 28 (1989) 347.
[21] R. Alcala, J.W. Shabaker, G.W. Huber, M.A. Sanchez-castillo, J.A. Dumesic, J. Phys. Chem. B 109 (2005) 2074.
[22] E. Zahidi, M. Castonguay, P. McBreen, J. Am. Chem. Soc. 116 (1994) 5847.
[23] E. Zahidi, M. Castonguay, P.H. McBreen, J. Phys. Chem. 99 (1995) 17906.
[24] K.I. Gursahani, R. Alcala, R.D. Cortright, J.A. Dumesic, Appl. Catal. A: Gen. 222 (2001) 369.
[25] F. Calaza, D. Stacchiola, M. Neurock, W.T. Tysoe, Surf. Sci. 598 (2005) 263.
[26] Z.J. Li, F. Calaza, C. Plaisance, M. Neurock, W.T. Tysoe, J. Phys. Chem. C 113 (2009) 971.
[27] C.M. Horiuchi, M. Rangan, B.M. Israel, J.W. Medlin, J. Phys. Chem. C 113 (2009) 14900.
[28] C.M. Horiuchi, J.W. Medlin, Surf. Sci. 604 (2010) 98.
[29] J.W. Medlin, C.M. Horiuchi, M. Rangan, Top. Catal. 53 (2010) 1179.
[30] P. Mäki-Arvela, I. Kubickova, M. Snåre, K. Eränen, D.Y. Murzin, Energy Fuels 21 (2007) 30.
[31] R.D. Haley, M.S. Tikhov, R.M. Lambert, Catal. Lett. 76 (2001) 125.
[32] A.K. Agarwal, N.W. Cant, M.S. Wainwright, D.L. Trimm, J. Mol. Catal. 43 (1987) 79.
[33] L. Xu, Y. Xu, Surf. Sci. 604 (2010) 887.
[34] R. Alcala, M. Mavrikakis, J.A. Dumesic, J. Catal. 218 (2003) 178.
[35] H.F. Wang, Z.P. Liu, J. Am. Chem. Soc. 130 (2008) 10996.
[36] M. Li, W. Guo, R. Jiang, L. Zhao, H. Shan, Langmuir 26 (2010) 1879.
[37] D.W. Goodman, J.T. Yates, J. Catal. 82 (1983) 255.
[38] E. Ozensoy, B.K. Min, A.K. Santra, D.W. Goodman, J. Phys. Chem. B 108 (2004) 4351.
[39] T. Zubkov, J. Morgan, A. Gregg, J.T. Yates Jr., Chem. Phys. Lett. 362 (2002) 181.
[40] H. Dietrich, P. Geng, K. Jacobi, G. Ertl, J. Chem. Phys. 104 (1996) 375.
[41] S. Dahl, A. Logadottir, R.C. Egeberg, J.H. Larsen, I. Chorkendorff, E. Tornqvist, J.K. Nørskov, Phys. Rev. Lett. 83 (1999) 1814.
[42] W.F. Banholzer, R.I. Masel, J. Catal. 85 (1984) 127.
[43] J.M. Gohndrone, R.I. Masel, Surf. Sci. 209 (1989) 44.
[44] T. Zambelli, J. Wintterlin, J. Trost, G. Ertl, Science 273 (1996) 1688.
[45] D.W. Goodman, Surf. Sci. 123 (1982) L679.
[46] D.W. Goodman, Catal. Today 12 (1992) 189.
[47] T.P. Beebe, D.W. Goodman, B.D. Kay, J.T. Yates, J. Chem. Phys. 87 (1987) 2305.
[48] J.K. Nørskov, T. Bligaard, A. Logadottir, S. Bahn, M. Bollinger, L.B. Hansen, H. Bengaard, B. Hammer, Z. Sljivancanin, M. Mavrikakis, Y. Xu, S. Dahl, C.J.H. Jacobsen, J. Catal. 209 (2002) 275.
[49] Z.P. Liu, P. Hu, J. Am. Chem. Soc. 125 (2003) 1958.
[50] K. Honkala, A. Hellman, I.N. Remediakis, A. Logadottir, A. Carlsson, S. Dahl, C.H. Christensen, J.K. Nørskov, Science 307 (2005) 555.
[51] Q. Ge, M. Neurock, J. Am. Chem. Soc. 126 (2004) 1551.
[52] Y. Xu, M. Mavrikakis, Surf. Sci. 538 (2003) 219.
[53] Y. Xu, M. Mavrikakis, J. Phys. Chem. B 107 (2003) 9298.
[54] P. Christopher, S. Linic, J. Am. Chem. Soc. 130 (2008) 11264.
[55] P. Christopher, S. Linic, ChemCatChem 2 (2010) 78.
[56] M.S. Chen, D. Kumar, C.-W. Yi, D.W. Goodman, Science 310 (2005) 291.
[57] P. Han, S. Axnanda, I. Lyubinetsky, D.W. Goodman, J. Am. Chem. Soc. 129 (2007) 14355.
[58] G. Kresse, J. Hafner, Phys. Rev. B 47 (1993) 558.
[59] G. Kresse, J. Hafner, Phys. Rev. B 49 (1994) 14251.
[60] G. Kresse, J. Furthmüller, Comput. Mater. Sci. 6 (1996) 15.
[61] J.P. Perdew, K. Burke, M. Ernzerhof, Phys. Rev. Lett. 77 (1996) 3865.
[62] G. Kresse, J. Joubert, Phys. Rev. B 59 (1999) 1758.
[63] M. Methfessel, A.T. Paxton, Phys. Rev. B 40 (1989) 3616.
[64] P.E. Blöchl, O. Jepsen, O.K. Andersen, Phys. Rev. B 49 (1994) 16223.
[65] N.W. Ashcroft, N.D. Mermin, Solid State Physics, Saunders College, Orlando, FL, 1976.
[66] G. Henkelman, H. Jónsson, J. Chem. Phys. 113 (2000) 9978.
[67] G. Henkelman, B.P. Uberuaga, H. Jónsson, J. Chem. Phys. 113 (2000) 9901.
[68] G. Henkelman, H. Jónsson, J. Chem. Phys. 111 (1999) 7010.
[69] R.A. Olsen, G.J. Kroes, G. Henkelman, A. Arnaldsson, H. Jónsson, J. Chem. Phys. 121 (2004) 9776.
[70] A. Heyden, A.T. Bell, F.J. Keil, J. Chem. Phys. 123 (2005) 224101.
[71] V. Pallassana, M. Neurock, J. Catal. 209 (2002) 289.
[72] Z.X. Chen, K.M. Neyman, K.H. Lim, N. Rosch, Langmiur 20 (2004) 8068.
[73] R.B. Jiang, W.Y. Guo, M. Li, D.L. Fu, H.H. Shan, J. Phys. Chem. C 113 (2009) 4188.
[74] K.H. Lim, Z.X. Chen, K.M. Neyman, N. Rosch, J. Phys. Chem. B 110 (2006) 14890.
[75] B. Hammer, L.B. Hansen, J.K. Nørskov, Phys. Rev. B 59 (1999) 7413.
[76] M. Gajdos, A. Eichler, J. Hafner, J. Phys.: Conds. Matter 16 (2004) 1141.
[77] J.L. Davis, M.A. Barteau, J. Am. Chem. Soc 111 (1989) 1782.
[78] J.L. Davis, M.A. Barteau, Surf. Sci 235 (1990) 235.
[79] B. Hammer, J.K. Nørskov, Adv. Catal. 45 (2000) 71.
[80] V. Pallassana, M. Neurock, L.B. Hansen, B. Hammer, J.K. Nørskov, Phys. Rev. B 60 (1999) 6146.
[81] D. Loffreda, D. Simon, P. Sautet, J. Chem. Phys. 108 (1998) 6447.
[82] A. Michaelides, Z.P. Liu, C.J. Zhang, A. Alavi, D.A. King, P. Hu, J. Am. Chem. Soc. 125 (2003) 3704.
[83] P. Ferrin, D. Simonetti, S. Kandoi, E. Kunkes, J.A. Dumesic, J.K. Nørskov, M. Mavrikakis, J. Am. Chem. Soc. 131 (2009) 5809.
[84] F. Studt, F. Abild-Pedersen, T. Bligaard, R.Z. Sorensen, C.H. Christensen, J.K. Nørskov, Science 320 (2008) 1320.
[85] A. Logadottir, T.H. Rod, J.K. Nørskov, B. Hammer, S. Dahl, C.J.H. Jacobsen, J. Catal. 197 (2001) 229.
[86] H. Olcay, L. Xu, Y. Xu, G.W. Huber, ChemCatChem 2 (2010) 1420.